

V.J. LOGEESWARAN¹
A.N. STAMEROFF¹
M. SAIF ISLAM^{1,✉}
W. WU²
A.M. BRATKOVSKY²
P.J. KUEKES²
S.Y. WANG²
R.S. WILLIAMS²

Switching between positive and negative permeability by photoconductive coupling for modulation of electromagnetic radiation

¹ Department of Electrical and Computer Engineering, University of California, Davis, CA 95616, USA
² Quantum Science Research Group, Hewlett Packard Laboratories, Palo Alto, CA 94304, USA

Received: 27 October 2006/Accepted: 19 January 2007
Published online: 3 March 2007 • © Springer-Verlag 2007

ABSTRACT We introduce a modulation mechanism for negative index materials (NIM) in the GHz frequency range by means of photoconductive coupling. This leads the way to a monolithically integrated modulable NIM achieved by conventional microfabrication techniques. The photosensitive material is deposited in the gap of the split ring resonator (SRR) structure and the response in terms of S-parameters is simulated using a high frequency structure simulator (HFSSTM) program. Only a single SRR particle is simulated to demonstrate total suppression of resonance amplitude and without any loss of generality the concept is applicable to a NIM comprising of both negative permeability and negative permittivity. This simple modulation of refractive indices can lead to novel optical device developments with the potential to dramatically improve the performance of existing phased array antennas, optical beam-forming networks, antenna remoting and transportation of RF power through fiber.

PACS 42.60.Fc; 42.82.Cr; 81.05; 73.50.Pz

1 Introduction

Interest in the field of artificial electromagnetic materials has been growing phenomenally since the “discovery” of materials that have been termed metamaterials (MTM), also known as negative index material (NIM), double negative media (DNM), left-handed media (LHM), backward wave media (BWM), and negative refractive index media (NRI). These metamaterials are a new class of materials that exhibit unique properties that are consistent with simultaneous negative permittivity ($\epsilon < 0$) and negative permeability ($\mu < 0$) as postulated by Veselago [1]. Since the first experimental verification of its existence by Smith, Shelby, Pendry and coworkers [2–5] in the 1–10 GHz frequency range, many other groups have pushed the demonstration to THz, IR and visible frequencies [6–11]. The widely accepted concept in synthesizing NIM is to construct a composite periodic array of particles comprising: magnetic resonant particles e.g. split-ring resonator (SRR) that is ideally excited by the magnetic fields (H-field) and conducting particles e.g. cut-wires, that are ideally excited by the electric fields (E-field). The dimensions of these particles should be much smaller than the

wavelength of interest ($a \sim \lambda/10$), such that, the incident electromagnetic radiation ‘sees’ a homogeneous material during the wave–material interaction.

Applications of NIM in perfect lens, filters and couplers have been very promising [12–17]. It would be of great interest to extend the application domain to incorporate NIM based devices at microwave/optical frequencies that are tunable and can be modulated optically. Photoconductive effects refer to the modulation of resistance (conductance) of a material under optical illumination because of the photo-generation of carriers. Illumination of photoconductive materials by a short ultra-fast optical pulse of reasonable power can produce these carriers. This process is governed by optical generation, electrical transport and recombination of carriers. Therefore, material selection and fabrication processes become critical. Use of photoconductive materials in microwave circuits can be traced back to pioneering works of Sommers and Teutsch [18] who investigated the demodulation of broadband optical signals with RF biased photodetectors. Since then many researchers have devised instruments and sensors by exploiting semiconductor photoconductivity phenomenon to control microwave transmission and propagation [19–22].

In the nascent field of NIM, there were earlier efforts by Djemoun et al. [23] to introduce tunability to NIM by attaching pin diodes to their metamaterial structure and thus switching the permittivity parameter. Lee et al. [24] and K. Aydin et al. [25] proposed a tunable SRR by inserting lumped inductors and capacitors in the split-gap of the SRR. The approaches adopted by these groups were mainly in hybrid integration of the tuning element. More recently Padilla et al. [26] have successfully demonstrated a dynamic metamaterial at THz frequencies using photo-generated free carriers in the semi-insulating GaAs substrate patterned with the SRR particles. The optical excitation was done using a 50 fs 800 nm pulse laser and the switching response was mainly limited by the recombination time of the free-carriers in GaAs to ~ 1 ns. Their approach is probably the first monolithic integration of the tuning element, i.e. the GaAs substrate with the NIM particles. Hence the drive for monolithic integration, especially at higher frequencies, is growing.

In the following sections, the approach for modulating NIM using photoconductive coupling to a SRR will be described. Section 2 provides the approach method and model for the development of the photo-modulation and the influ-

✉ Fax: 530-752-8428, E-mail: saif@ece.ucdavis.edu

ence of the bi-anisotropic nature of the SRR on the propagation direction and resonance modes. In Sect. 3, the simulation model and results are discussed. Section 4 details the low cost process steps and fabrication issues that are currently being addressed in order to realize the modulation of negative effective permeability (SRR) structures on a monolithically integrated Si wafer. A feasible scheme for application of index modulation in a modulator and its system application will also be briefly presented.

2 Method

A general schematic showing the various regimes in the electromagnetic–material interaction is shown in Fig. 1 adapted from [15]. In this paper, the modulation mechanism discussed is confined to that of switching the permeability parameter of the SRR between the 2nd (electrical plasma) and the 3rd-quadrant (NIM). Modulation is achievable for NIM ($\epsilon < 0$ and $\mu < 0$)-3rd quadrant, by switching between the quadrants either ($\epsilon < 0$ and $\mu > 0$)-2nd quadrant or ($\epsilon > 0$ and $\mu < 0$)-4th quadrant or ($\epsilon > 0$ and $\mu > 0$)-1st quadrant. It is assumed that the placement of the cut-wire ($\epsilon < 0$) with respect to the SRR particles is judiciously chosen to minimize the undesired interaction between the magnetic responses of the cut-wire with the SRR. This would ensure that the magnetic response is sensitive to changes in the SRR material and not to the cut-wires.

A typical SRR structure is shown in Fig. 2. It comprises of two concentric rings with a split-gap between the otherwise continuous rings and a radial gap between the two rings. The two split rings are resonators coupled by common magnetic flux (mutual inductance) and mutual capacitance. The SRR particle is inherently bi-anisotropic and hence the desired resonance mode excitation via E-field and/or H-field must be both considered. The presence of the inner ring is to decrease the SRR resonance frequency in the fundamental magnetic mode and to reduce the magnetoelectric coupling effects such that the contribution of the E-field to the fundamental magnetic mode is kept to a minimum. In NIM applications, the substrate, the split-gap or the radial gap can be made of photo-

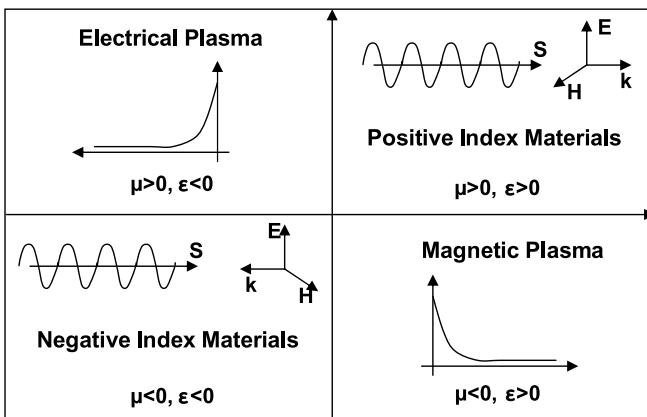


FIGURE 1 A compact depiction of the different regimes of electromagnetic wave–material interaction, adapted from [15]. Modulation is achievable for NIM ($\epsilon < 0$ and $\mu < 0$)-3rd quadrant, by switching between the quadrants i.e., if either ($\epsilon < 0$ and $\mu > 0$)-2nd quadrant or ($\epsilon > 0$ and $\mu < 0$)-4th quadrant or both ($\epsilon > 0$ and $\mu > 0$)-1st quadrant

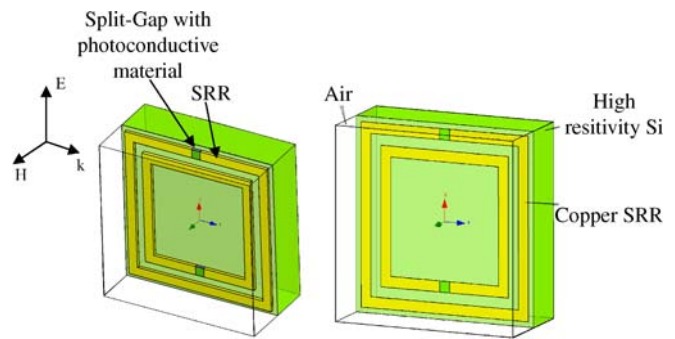


FIGURE 2 SRR model showing the parts and the material parameter definition used in the HFSS™ simulation. The dimensions of the particle are: SRR gap size = 60 μm , copper thickness = 20 μm , radial gap = 60 μm , substrate thickness = 500 μm , width of SRR metal = 60 μm , gap SiO_2 thickness = 18 μm , gap Si thickness = 2 μm and air encapsulation = 500 μm

conductive material suitable for excitation in the wavelength of interest. In our simulation the gap material is made from a bi-layer of 18 μm SiO_2 and 2 μm silicon. The metal was copper with thickness of 20 μm , while the substrate is high resistivity silicon (HRS), $\rho = 10 \text{ k}\Omega \text{ cm}$.

The SRR can be orientated in 4 different ways [26–28] with respect to the incoming propagation wave. The unit-cell fixed coordinate system xyz is as shown in Fig. 2. The resonance response to the two orientations shown in Fig. 3 is shown in the simulation section. For our purposes only the first configuration was chosen to highlight the variation in the SRR response corresponding to the photoconductivity changes of 0.01 S/m, 10 S/m, 100 S/m, 500 S/m, 6000 S/m and 10 kS/m. From Fig. 3, orientation A, the H-field will excite the magnetic resonance mode thereby inducing a circulatory current to flow in the rings and the E-field will excite the higher electrical resonance. Due to the bi-anisotropic nature, the H-field will also create the electric dipole response (in the k -direction) in the SRR at the same frequency as the magnetic response. This contribution is weak due to the opposing rings. For orientation B, there is a strong electrical response and a strong magnetic response at the same frequency.

When the split gaps (or radial gaps where a large field augmentation crops up) are shorted due to the conductivity changes from extra carrier generation, the rings are no longer capacitively and inductively coupled. This destroys

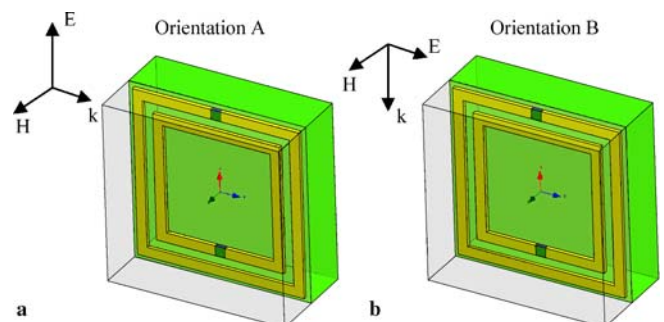


FIGURE 3 SRR model showing the orientation of the SRR unit cell and the wave propagation direction in the HFSS™ simulation. In (a) the E-field is polarized parallel to the split-gap while in (b) the E-field is polarized perpendicular to the split-gap. Both models have the H-field perpendicular to the plane of the SRR

the magnetic and electric resonance mode and the SRR no longer operates in the negative permeability regime [29]. The conductivity changes are assumed to originate from the optically generated carriers in the photoconductor. The absorption length of the sample should be \sim the skin depth for effective response. The photo-induced electron–hole plasma in a semiconductor interacts with the EM wave (by switching the SRR into a closed metal loop which is not a resonant structure for the frequency under consideration) thus modulating the permeability between negative and positive values when the electron–hole plasma reaches an appropriate level.

The electron–hole plasma in the layer with an absorption thickness of d , creates a complex permittivity in the plasma region, which can be expressed as [33]

$$\begin{aligned}\varepsilon_r &= \varepsilon' - j\varepsilon'', \\ &= \varepsilon_L - \frac{\omega_p^2}{\omega^2 + \nu^2} - j\frac{\nu}{\omega} \frac{\omega_p^2}{\omega^2 + \nu^2},\end{aligned}\quad (1)$$

where ω is the angular frequency of the RF field, ε_L = dielectric constant of host lattice, ν = carrier collision frequency and ω_p = plasma frequency, given by $\omega_p = \frac{n(t)e^2}{\varepsilon_0 m^*}$. The density of the photo-induced excess carriers proportional to laser intensity is given by n . For low frequency ($\sim < 20$ GHz), the photo-induced carrier will not significantly affect the real part of the complex permittivity and therefore the effective conductivity becomes

$$\sigma_{\text{eff}} = \omega \varepsilon_0 \varepsilon'' = n(t) e \mu. \quad (2)$$

For higher frequency operation, the real part has to be taken into account as the plasma exhibits increasingly dielectric behavior. The optical modulation signal can be selected based on the bandgap and absorption spectra of the photoconductive material. The carrier generation can be as large as 10^{20} cm^{-3} , for a laser with a wavelength of 500 nm and an intensity of $\sim 4 \text{ mW/cm}^2$. This translates to a conductivity of about a few thousand S/m. For fast switching response one has to consider the photo-carrier lifetime as well which can be in the order of nanoseconds. The method we employed by which the constitutive parameters were extracted for metamaterial displaying negative refractive index properties involve retrieving the scattering (S) parameters. The latter mentioned parameters are derived from a software simulation program Ansoft's High Frequency Structure Simulator (HFSSTM).

These properties are best characterized by the constitutive parameters of the structure, namely its effective permittivity (ε) and permeability (μ). The use of a split ring resonator structure achieves the goal of a metamaterial with constitutive parameters characteristic of left handed materials. Focusing our attention to an analysis involving a one dimensional approach, though higher dimensional structures can be constructed and utilized, we extracted constitutive parameters from the aforementioned S parameters. It is known that:

$$\varepsilon = n/z, \quad (3a)$$

$$\mu = nz, \quad (3b)$$

where n is the refractive index and z is the wave impedance [32]. Also, since we are considering a one dimensional

slab the transfer matrix has the form:

$$T = [\cos(nkd), -z/k \sin(nkd); k/z \sin(nkd), \cos(nkd)], \quad (4)$$

where k is the propagation constant of the incident electromagnetic wave. The S-parameters and the T-matrix are related as follows:

$$S_{11} = (T_{11} - T_{22} + \{jkT_{12} - T_{21}/jk\}) / (T_{11} + T_{22} + \{jkT_{12} + T_{21}/jk\}), \quad (5a)$$

$$S_{21} = 2 / (T_{11} + T_{22} + \{jkT_{12} + T_{21}/jk\}), \quad (5b)$$

$$S_{22} = (T_{22} - T_{11} + \{jkT_{12} - T_{21}/jk\}) / (T_{11} + T_{22} + \{jkT_{12} + T_{21}/jk\}). \quad (5c)$$

Also for a one dimensional slab we observe that:

$$S_{11} = S_{22}, \quad (6a)$$

$$S_{12} = S_{21}. \quad (6b)$$

Solving (2), (3b), and (4) we obtain the expressions for z and n :

$$z = \pm \sqrt{[(1 + S_{11})^2 - S_{21}^2] / [(1 - S_{11})^2 - S_{21}^2]}, \quad (7)$$

$$n = 1 / (kd) \ln \{X \pm j\sqrt{1 - X^2}\}, \quad (8)$$

where k is the propagation constant for the electromagnetic wave in free space, d is the width of the unit cell, and $X = (1/S_{21})(1 - S_{11}^2 + S_{21}^2)$. Taking (5c), (6b) and (1) we find values for the constitutive parameters that are frequency dependent. Namely, we derive permittivity and permeability for this structure as a function of frequency.

3 Simulation results

In our approach we employ an analysis method on a single split ring resonator (SRR) unit cell as seen in Fig. 2 and described in [30–32, 34]. Such a structure is shown to have negative permeability properties for certain wavelengths of incident electromagnetic radiation. To this end, we perused the SRR dimensions described in [34] and simulated the presence of optically generated carriers by changing the conductivity values of the slab that filled the SRR split gap. The model and the transmission scattering parameter S_{21} are shown in Fig. 4. The behavior is as expected, since the conductivity increases, the SRR loses its capacitive coupling and hence the transmission bandstop ($\mu < 0$) is extinguished.

Section 2 details the assumptions made in this approximation. Validation of the technique leads us to undertake simulation of a physically realizable unit cell (as shown in Fig. 2) whose left-handed capability can be modulated by an outside source of electromagnetic radiation. The starting conductivity value for the photoconductor was 0.01 S/m corresponding to high resistivity silicon (HRS). The frequency sweep was done in steps of 100 MHz. The HFSSTM simulated S-parameter magnitude; refractive index, permittivity, and permeability are all shown in Fig. 5. Applying the same analysis to this SRR unit cell we explore the capabilities of this structure and finally discuss some of its applications.

From Figs. 5 and 6, the magnetic response between 12–15 GHz is indeed characteristic of negative permeability. The actual operating frequency should be chosen such

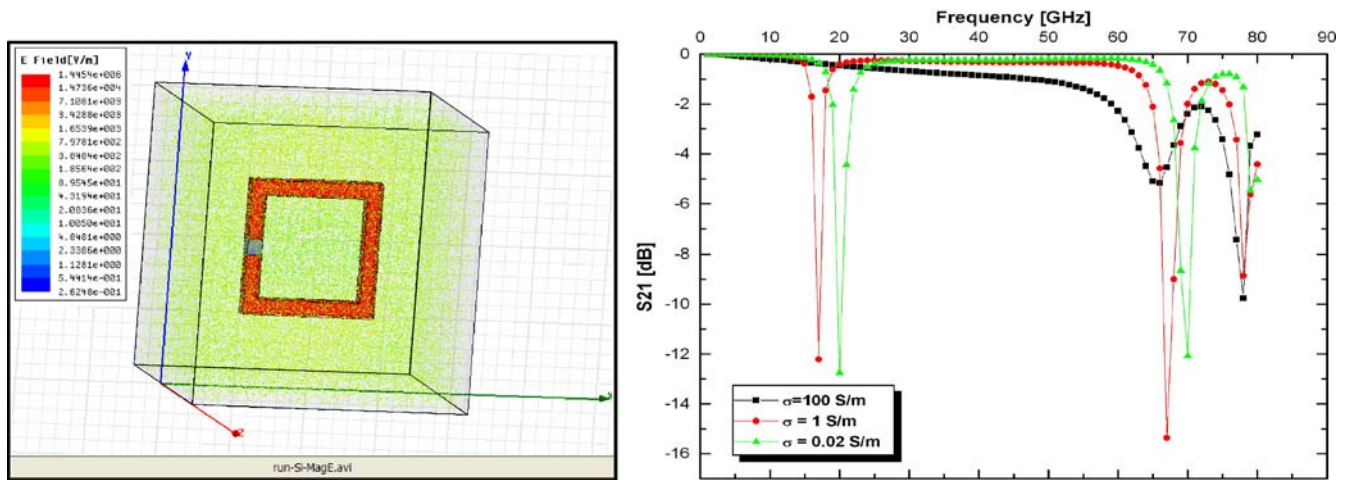


FIGURE 4 (a) SRR model showing the orientation of the SRR unit cell suspended in vacuum; (b) the transmission curves S_{21} clearly shows the extinction of the magnetic resonance at 20 GHz (see [34] for details on SRR structure and excitation polarization) as the conductivity of the split gap material is varied from 0.02 S/m, 1 S/m and 100 S/m. Note that the resonant frequency undergoes a shift

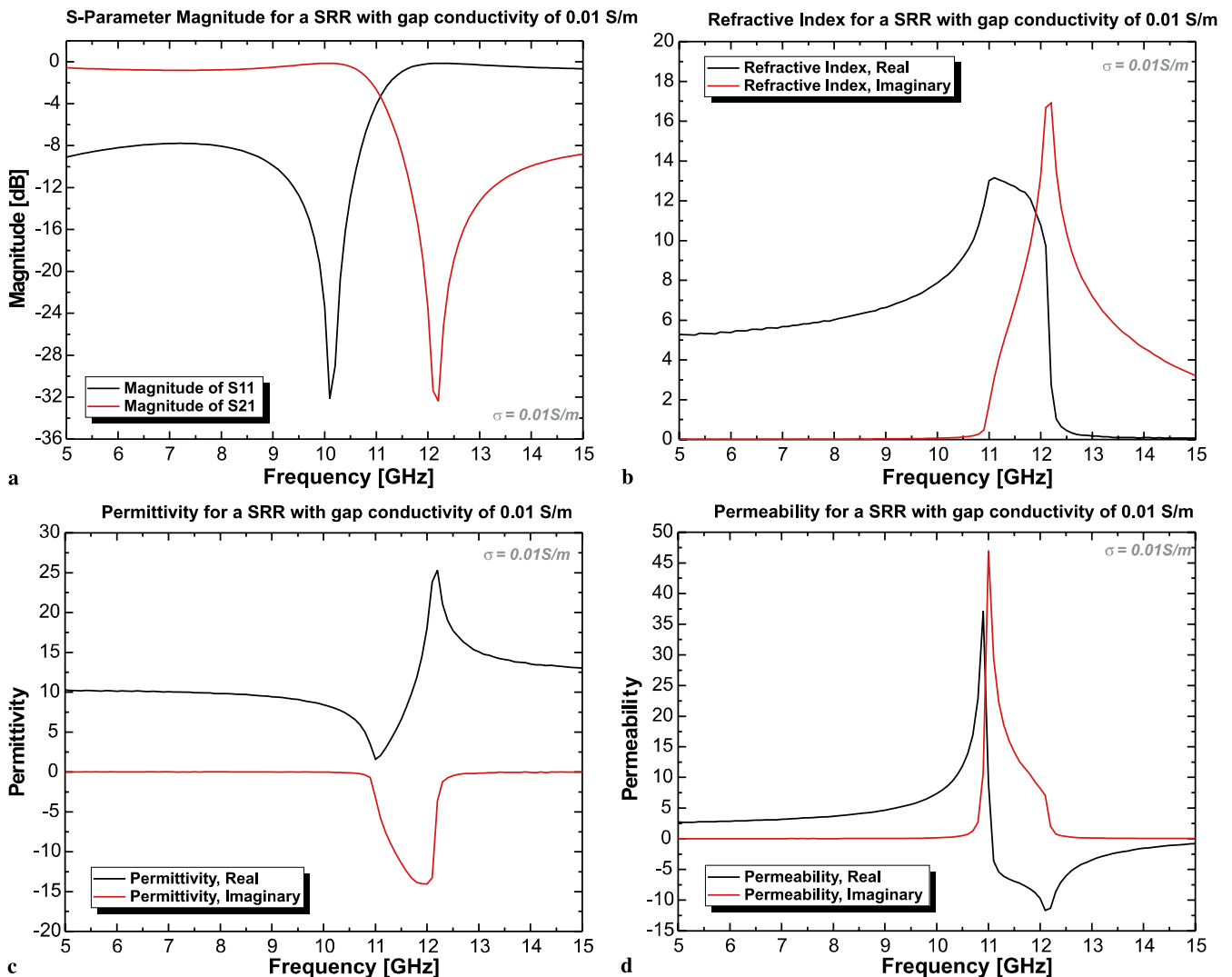


FIGURE 5 Orientation A: (a) S-parameters magnitude, (b) refractive index, (c) relative permittivity, and (d) relative permeability for the SRR structure shown in Fig. 2. The frequency interval was 100 MHz

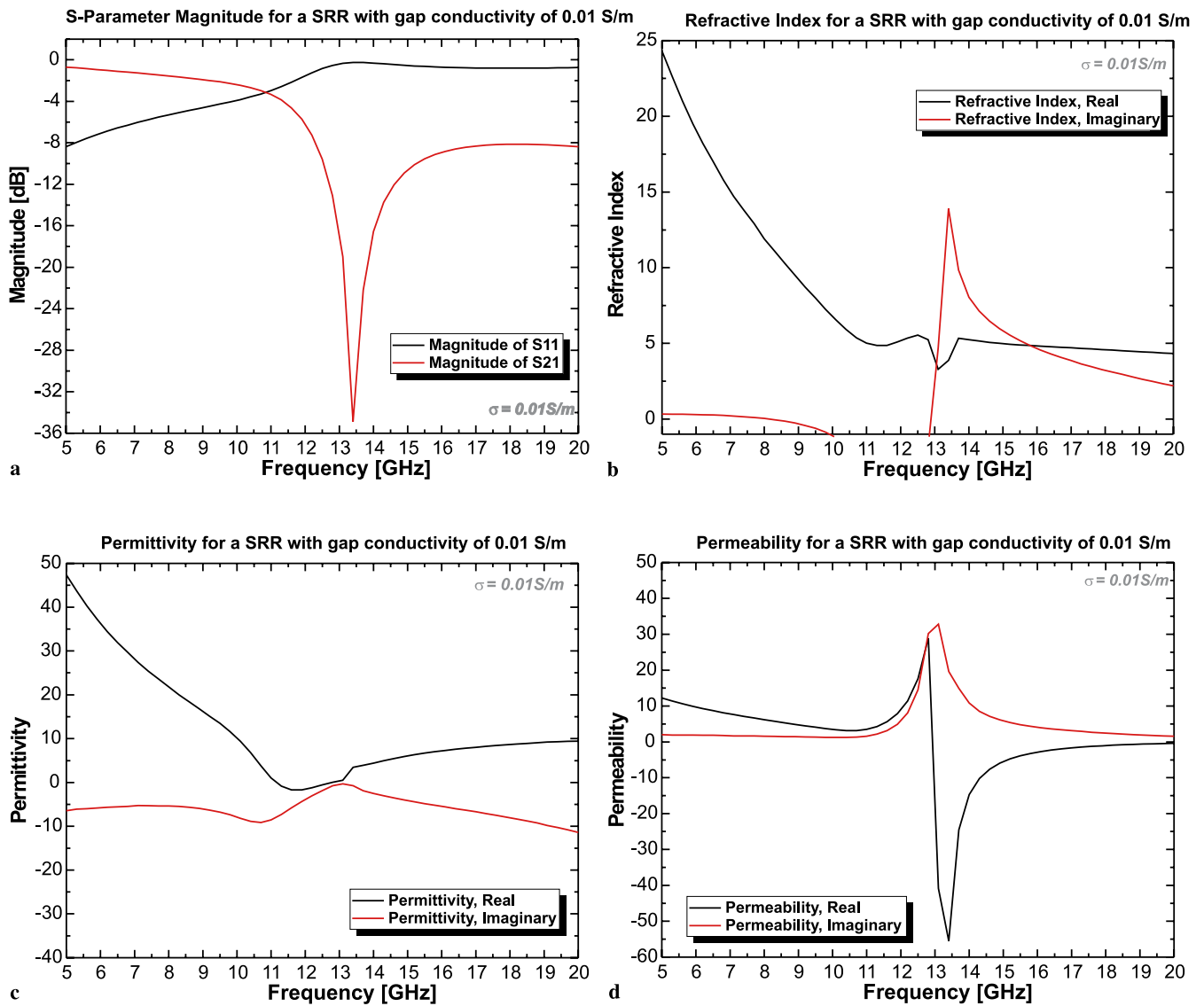
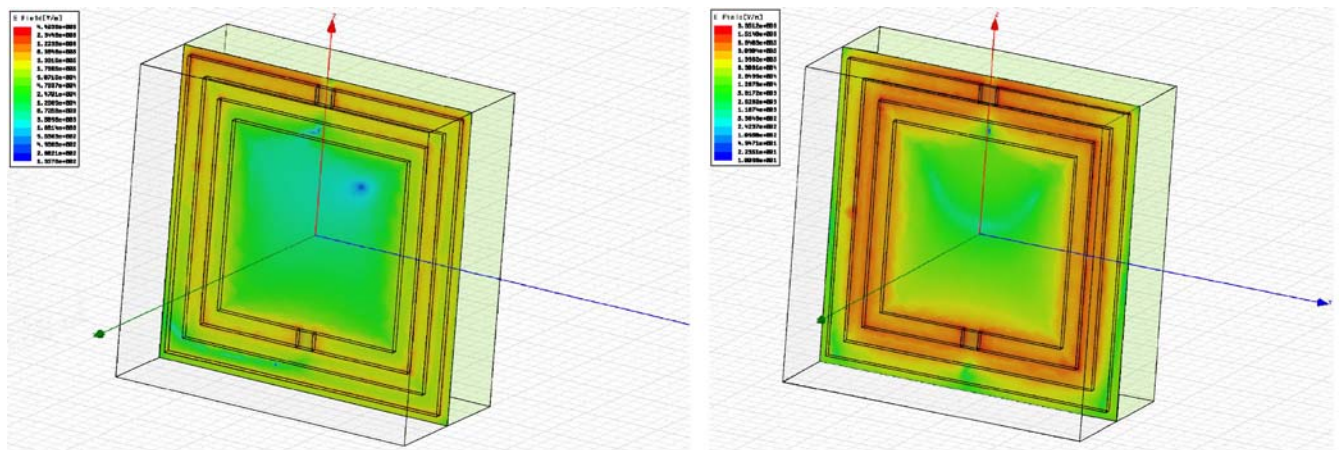
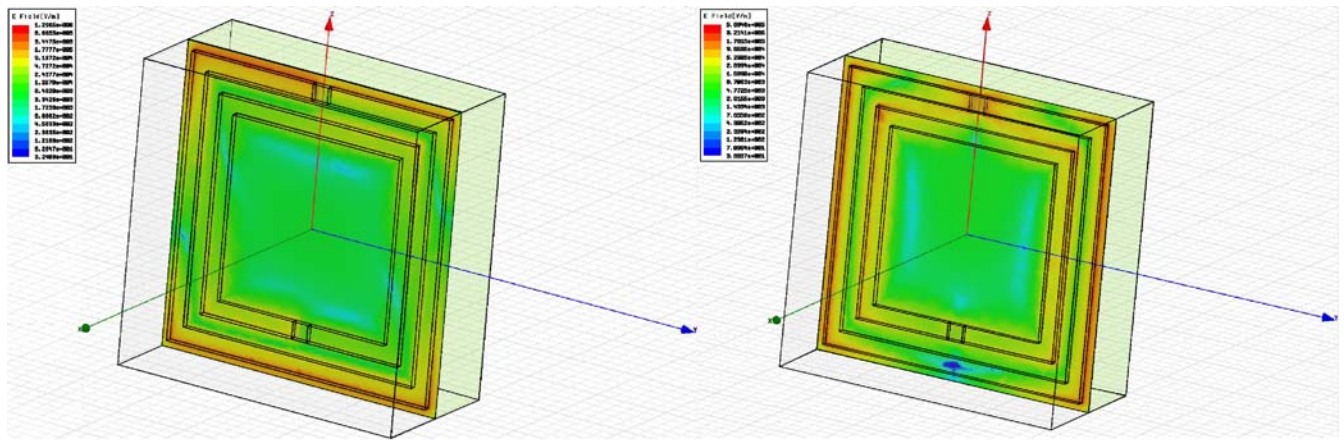


FIGURE 6 Orientation B: (a) S-parameters magnitude, (b) refractive index, (c) relative permittivity, and (d) relative permeability for the SRR structure shown in Fig. 2. The frequency interval was 300 MHz



Orientation A: E-field plot of the magnetic response at 14GHz with $\sigma=10$ S/m. Orientation B: E-field plot of the magnetic response at 14GHz with $\sigma=10$ S/m.
 FIGURE 7 (a) Electric field plot (log scale) showing the H-field excited magnetic resonance with a negligible electric response, (b) electric field plot (log scale) showing the H-field and E-field excited magnetic resonance with a non-negligible electric response



Orientation A: E-field plot of the magnetic response at 14GHz with $\sigma=10k$ S/m.

Orientation B: E-field plot of the magnetic response at 14GHz with $\sigma=10k$ S/m.

FIGURE 8 (a) Electric field plot (log scale) showing the loss of H-field excited magnetic resonance, (b) electric field plot (log scale) showing the loss of H-field and E-field excited magnetic resonance. The SRR now has become a closed split ring resonator (CSRR)

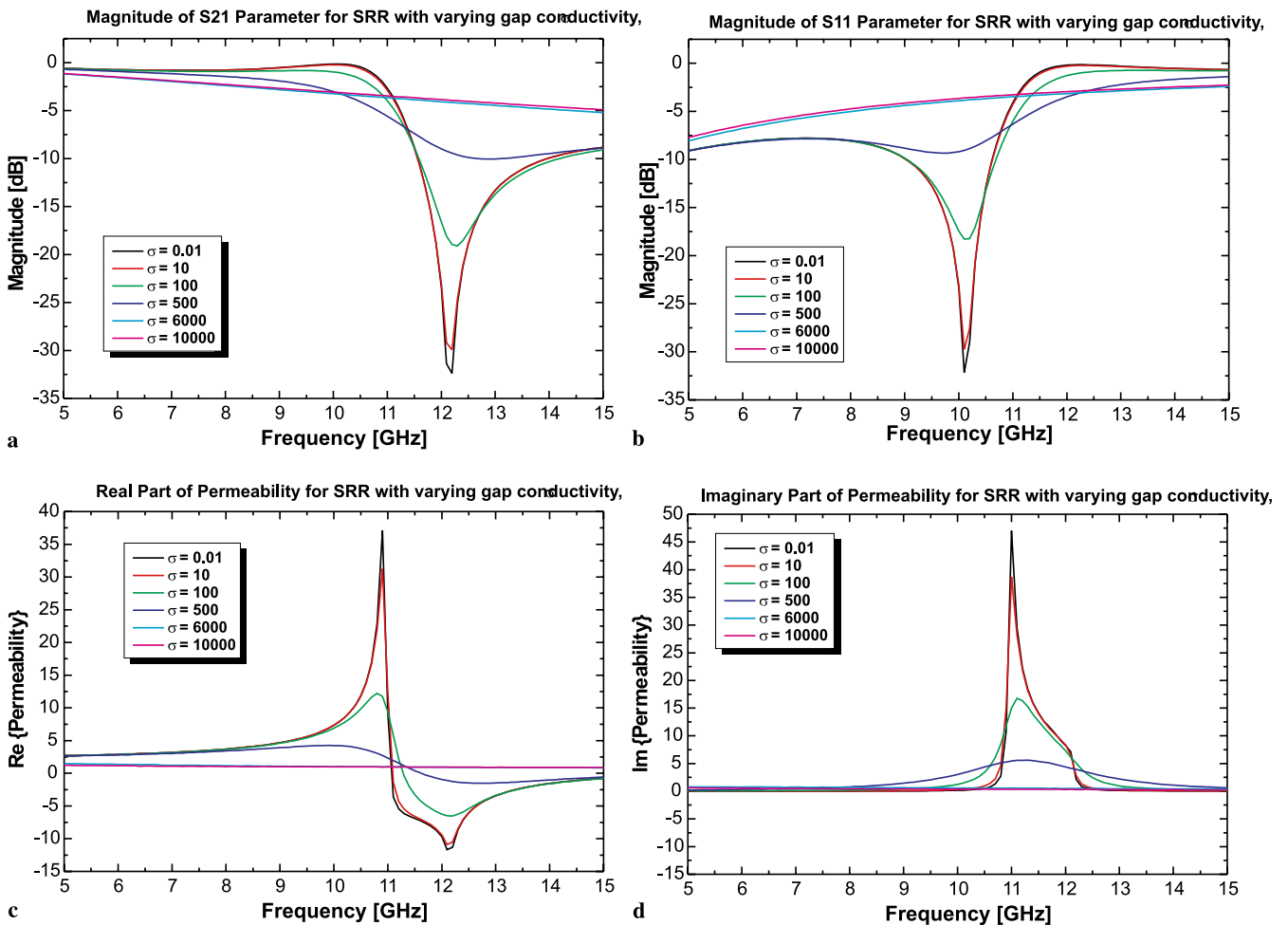


FIGURE 9 Orientation A: Comparison of the (a) S-parameters S21, (b) S11, (c) real part of permeability, and (d) imaginary part of permeability for the SRR structure shown in Fig. 2, with varying gap conductivity from photo-generated carrier concentration

that the losses are kept to a minimum for example at 14 GHz the effective permeability is given by $\mu_{eff} = (1.08 + j0.035)$. The difference in the SRR response due to two configurations A and B are also evident. The bi-anisotropic behavior of the SRR must be taken into account when deciding on the photo-modulation mechanism since the electric field

coupling is much larger compared to the magnetic field coupling.

Figure 7 gives a quantitative understanding of the resonance enhancement that exists in configuration B. If one is only interested in the magnetic response and not the electric response at the fundamental frequency then orientation A would

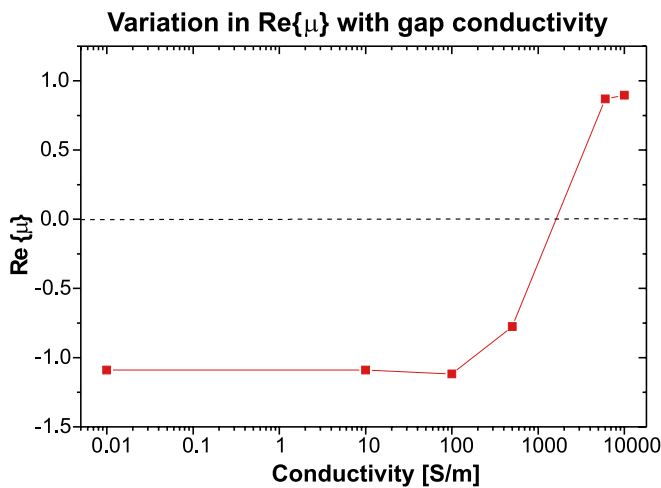


FIGURE 10 Orientation A: Comparison of the variation in the effective real permeability for varying conductivities at 14 GHz from photo-generated carrier concentration (*lines* drawn for clarity). The conductivity range between 500 S/m to 6000 S/m provides a window for operating in the switching mode. Simulation with finer variation in conductivity may reveal a better physical insight

be preferable. Based on the field intensity plot of Fig. 7b, besides shorting the split gap, the radial gap can also be modulated, although the focusing of the optical signal might be more challenging for the entire SRR cell and a high power optical source might be needed for such a flood exposure. In Fig. 8, upon photo-doping, the conductivity of the split gap material increases and this leads to a weakening of the mutual capacitive and inductive coupling between the inner and outer rings that dampens the magnetic resonance. Resistive losses then become dominant mainly due to the photo-carriers. The field also decreases by ~ 2 orders of magnitude. This is a clear indication of modulability of EM radiation with a large extinction ratio.

A comparison between the transmission (S21), reflective (S11), real and imaginary permeability for orientation A is shown in Fig. 9. The simulated effective photo-carrier in terms of variation in conductivity shows the diminishing resonant response as the carrier concentration is increased. The simulated values at 14 GHz are summarized in Fig. 10.

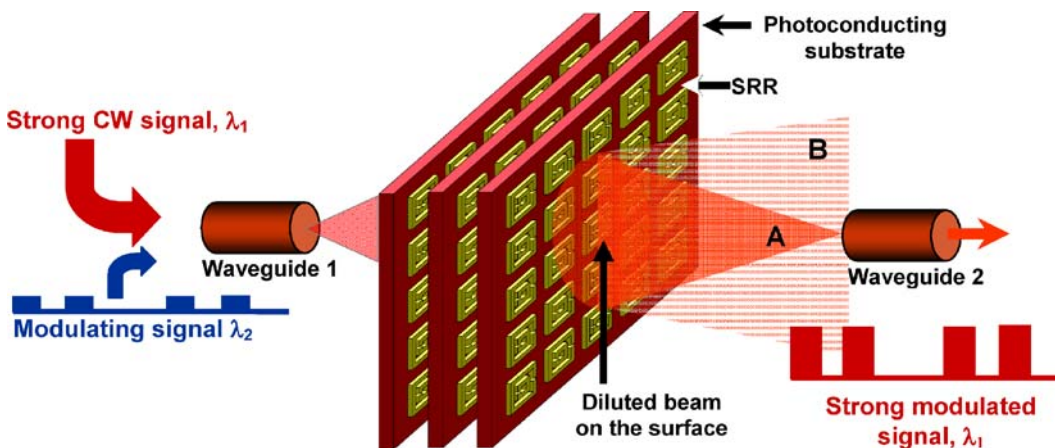


FIGURE 11 Schematics of a proposed modulator based on switching of indices of metamaterials. A high power signal (in red color) can be modulated by using a weak modulating signal (shown in blue) without running onto non-linearity by diverging the beam on the substrate. A and B indicate a focused and defocused high power beam. The weak modulating signal will not be transmitted to waveguide 2 due to absorption on the metamaterial substrate

Based on the switching of permeability of meta-materials, we propose a novel modulating device for modulation and switching of electromagnetic radiation. The proposed scheme is illustrated in Fig. 11. A high power cw signal with a wavelength λ_1 is focused from waveguide 1 to waveguide 2 using the focusing capability of metamaterials. The signal can be diluted on the metamaterial substrate which is fabricated using a highly resistive photo-conducting surface. The substrate can be chosen to remain transparent at λ_1 . An optical excitation of wavelength λ_2 can be employed to generate a large number of photo-carriers in the substrate which will short the SRRs, detuning the resonance of the metamaterial and causing the λ_1 -beam to lose convergence. This will, in turn, result in a negligible power coupling to waveguide 2 and will cause a large on-off ratio in the electromagnetic signal collected by the waveguide 2. The dilution of the λ_1 -beam will allow modulation of a high power beam without stumbling upon high non-linearity or thermal failure – common issues with most high power optical modulators. If high resistance Si substrate is chosen for fabricating metamaterials, any wavelength longer than $\lambda_g = 1.12 \mu\text{m}$ can be effectively modulated using this method. The modulating optical signal can be $\lambda < 1.12 \mu\text{m}$. The modulation speed will remain limited by the carrier generation-recombination lifetime and mobility in the substrate. Modulation of shorter wavelengths can be achieved by using GaAs ($\lambda_g = 0.87 \mu\text{m}$) or GaN ($\lambda_g = 400 \text{nm}$) substrates. The scheme will enable high speed modulation of a high power cw signal using a low power modulating signal of shorter wavelength. Modulation at ratio frequency will be relatively easier than that of an optical frequency because of the relative ease of fabrication of meta-materials operating at RF. Optical fiber can be effectively used as waveguides for optical frequencies and optical feeding can then be implemented via monolithic integration of optical waveguides to each SRR. High speed modulation can then be achieved using substrates with ultra-fast carrier transport characteristics.

4 Fabrication process

The fabrication process is depicted in Fig. 12. For thick metal deposition, electroplating is a suitable process. Microelectronics compatible fabrication processes including metal lift-off and deposition of dielectrics and photo-

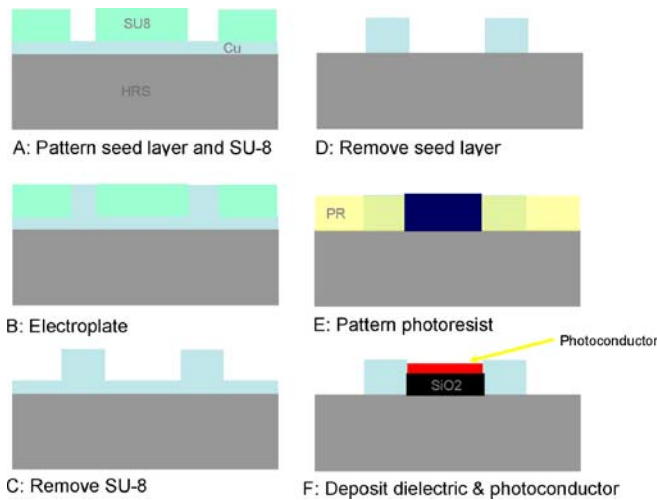


FIGURE 12 (a) The process is begun with a HRS substrate and patterned with SU8, (b) this forms the electroplating mold for Cu, (c) SU8 is then removed, (d) the seed layer for electroplating is then etched, (e) a thicker positive resist is spin-coated and patterned with areas exposed, (f) for the deposition of dielectric and photoconductor

conductors can help realize dynamically modulable metamaterials on a highly resistive silicon (Si) surface. Integration of an array of passive optical waveguides connected to the split gaps of an individual SRR unit offers a very efficient modulation scheme. Rather than flood-exposing the whole wafer with an intense optical beam, the proposed array of waveguides can minimize the overall optical power for photoconductive modulation. If III-V substrates are used for fabrication of NIM, on-chip integration of an active modulating laser diode connected to each SRR could be feasible.

5 Conclusion

We have discussed the photo-modulation effects of a SRR unit cell using specific analysis and simulation techniques. The approach for modulating NIM using photoconductive coupling to a SRR has been described and simulation results strongly suggests that this method of modulation is feasible. The theoretical model for the development of the photo-modulation and the influence of the bi-anisotropic nature of the SRR on the propagation direction and resonance modes were illustrated with a view to control, and carefully analyze, the electromagnetic response. The physical realization of the proposed monolithic SRR structure has also been detailed in the form of process steps. A new modulator based on photo induced index modulation is proposed and fabrication methods are discussed. Further experiments and more simulation are under way to demonstrate this modulation mechanism. Our results open exciting opportunities for novel devices such as optically controlled switches and modulators for applications in photonic and RF communication links.

ACKNOWLEDGEMENTS The authors would like to thank G. Medeiros-Ribiero, and E. Ponzovskaya, of HP Labs, the staff of Northern

California Nanofabrication Center (NCNC) in UC Davis and the meta-material team of HP Labs-UC Berkeley-UIUC-Duke University for helpful discussions. This work was supported by NSF CAREER grant #0547679, UC Davis research grant and a CITRIS grant sponsored by the Hewlett-Packard Company.

REFERENCES

- V.G. Veselago, *Sov. Phys. Uspekhi* **10**, 509 (1968)
- R.A. Shelby, D.R. Smith, S. Schultz, *Science* **292**, 77 (2001)
- D.R. Smith, W.J. Padilla, D.C. Vier, S.C. Nemat-Nasser, S. Schultz, *Phys. Rev. Lett.* **84**, 4184 (2000)
- J.B. Pendry, A.J. Holden, D.J. Robbins, W.J. Stewart, *IEEE Trans. Microw. Theory Technol.* **47**, 2057 (1999)
- J.B. Pendry, A.J. Holden, W.J. Stewart, I. Youngs, *Phys. Rev. Lett.* **76**, 4773 (1996)
- T.J. Yen, W.J. Padilla, N. Fang, D.C. Vier, D.R. Smith, J.B. Pendry, D.N. Basov, X. Zhang, *Science* **303**, 1494 (2004)
- C. Enkrich, M. Wegener, S. Linden, S. Burger, L. Zschiedrich, F. Schmidt, J. Zhou, T. Koschny, C.M. Soukoulis, *Phys. Rev. Lett.* **95**, 203901 (2005)
- H.O. Moser, B.D.F. Casse, O. Wilhelmi, B.T. Saw, *Phys. Rev. Lett.* **94**, 063901 (2005)
- S. Zhang, W.J. Fan, N.C. Panoiu, K.J. Malloy, R.M. Osgood, S.R.J. Brueck, *Phys. Rev. Lett.* **95**, 137404 (2005)
- V.M. Shalaev, W.S. Cai, U.K. Chettiar, H.K. Yuan, A.K. Sarychev, V.P. Drachev, A.V. Kildishev, *Opt. Lett.* **30**, 3356 (2005)
- T.F. Gundogdu, I. Tsiapa, A. Kostopoulos, G. Konstantinidis, N. Katsarakis, R.S. Penciu, M. Kafesaki, E.N. Economou, T. Koschny, C.M. Soukoulis, *Appl. Phys. Lett.* **89**, 084103 (2006)
- J.B. Pendry, *Phys. Rev. Lett.* **85**, 3966 (2000)
- N. Fang, H. Lee, C. Sun, X. Zhang, *Science* **308**, 534 (2005)
- A. Alù, N. Engheta, *IEEE Trans. Antennas Propag.* **51**, 2558 (2003)
- S.A. Ramakrishna, *Rep. Prog. Phys.* **68**, 449 (2005)
- N. Engheta, R.W. Ziolkowski, *IEEE Trans. Microw. Theory Technol.* **53**, 1535 (2005)
- C. Caloz, T. Itoh, *Electromagnetic Metamaterials: Transmission Line Theory and Microwave Applications* (Wiley, Hoboken, New Jersey, 2005)
- H.S. Sommers, W.B. Teutsch, *Proc. IEEE* **52**, 144 (1964)
- R.M. Arnold, F.J. Rosenbaum, *IEEE Trans. Electron. Dev.* **18**, (1971)
- K.E. Mortenson, A.L. Armstrong, J.M. Borrego, J.F. White, *Proc. IEEE* **59**, 1191 (1971)
- D.H. Auston, *Appl. Phys. Lett.* **26**, 3 (1975)
- A.M. Johnson, D.H. Auston, *IEEE J. Quantum Electron.* **QE-11**, 6 (1975)
- A. Djemoun, A. De Lustrac, F. Gadof, E. Akmansoy, In: *Epfl. Latsis NIM Symp.* (2005)
- S.W. Lee, Y. Kuga, A. Ishimaru, *Prog. Electromagn. Res. PIER* **51**, 219 (2005)
- K. Aydin, I. Bulu, K. Guven, M. Kafesaki, C.M. Soukoulis, E. Ozbay, *New J. Phys.* **7**, 168 (2005)
- W.J. Padilla, A.J. Taylor, C. Highstrete, M. Lee, R.D. Averitt, *Phys. Rev. Lett.* **96**, 107401 (2006)
- D.R. Smith, J. Gollub, J.J. Mock, W.J. Padilla, D. Schurig, *J. Appl. Phys.* **100**, 024507 (2006)
- P. Gay Balmaz, O.J.F. Martin, *J. Appl. Phys.* **92**, 2929 (2002)
- K. Aydin, K. Guven, N. Katsarakis, C.M. Soukoulis, E. Ozbay, *Opt. Express* **12**, 94 (2004)
- X. Chen, B.I. Wu, J.A. Kong, T.M. Grzegorzczuk, *Phys. Rev. E* **71**, 046610 (2005)
- D.R. Smith, S. Schultz, P. Markos, C.M. Soukoulis, *Phys. Rev. B* **65**, 195104 (2002)
- D.R. Smith, D.C. Vier, T. Koschny, C.M. Soukoulis, *Phys. Rev. E* **71**, 036617 (2005)
- C.H. Lee, *IEEE Trans. Microw. Theory Technol.* **38**, 596 (1990)
- M. Kafesaki, T. Koschny, R.S. Penciu, T.F. Gundogdu, E.N. Economou, C.M. Soukoulis, *J. Opt. A Pure Appl. Opt.* **7**, 12 (2005)